

High-bandwidth frequency domain multiplexed readout of transition-edge sensors for neutrinoless double beta decay searches

M. Adamić,^{a,b,*} M. Beretta,^{c,1} J. Camilleri,^{b,d} C. Capelli,^{b,2,*} M. A. Dobbs,^a T. Ellefot,^e B. K. Fujikawa,^b Yu. G. Kolomensky,^{b,c} D. Mayer,^f J. Montgomery,^a V. Novosad,^g A. M. Sindhwan,^{c,h} V. Singh,^c G. Smecher,ⁱ A. Suzuki,^e B. Welliver^c

^a*Department of Physics and Trottier Space Institute, McGill University, Montreal, QC H3A 2T8, Canada*

^b*Nuclear Science Division, Lawrence Berkeley National Laboratory, Berkeley, CA 94720, USA*

^c*Department of Physics, University of California Berkeley, Berkeley, CA 94720, USA*

^d*Center for Neutrino Physics, Virginia Polytechnic Institute and State University, Blacksburg, VA 24061, USA*

^e*Physics Division, Lawrence Berkeley National Laboratory, Berkeley, CA 94720, USA*

^f*Laboratory for Nuclear Science, Massachusetts Institute of Technology, Cambridge, MA 02139, USA*

^g*Materials Science Division, Argonne National Laboratory, Lemont, IL 60439, USA*

^h*Department of Nuclear Engineering, University of California Berkeley, Berkeley, CA 94720, USA*

ⁱ*t0.technology, Montreal, QC H2J 2L1, Canada*

E-mail: michel.adamic@mail.mcgill.ca, chiara.capelli@physik.uzh.ch

^{*}Corresponding author

¹Now at INFN Sezione di Milano-Bicocca, Milano, Italy

²Now at Physik-Institut, University of Zürich, 8057 Zürich, Switzerland

ABSTRACT: The next-generation of cryogenic neutrinoless double-beta decay experiments require increasingly fast readout in order to improve background discrimination. These experiments, operated as cryogenic calorimeters at ~ 10 mK, are usually read out by high-impedance neutron transmutation doped (NTD) thermistors, which provide good energy resolution, but are limited by ~ 1 ms response times. Superconducting detectors, such as transition-edge sensors (TESs) with a time resolution of ~ 100 μ s, offer superior timing performance over NTD semiconductor bolometers. To make this technology viable for an application to a thousand or more channels, multiplexed readout is necessary in order to minimize the thermal load and radioactive contamination induced by the readout. Frequency-domain multiplexing readout (fMux) for TESs, previously developed at Berkeley Lab and McGill University, is currently in use for mm-wave telescopes with detector sampling rates in the order of 100 Hz. We demonstrate a new readout system, based on the McGill/Berkeley digital fMux readout, to satisfy the higher bandwidth and noise requirements of the next generation of TES-instrumented cryogenic calorimeters. The new readout samples detectors at 156 kHz, three orders of magnitude faster than its cosmology-oriented predecessor. Each multiplexing readout module comprises ten superconducting resonators in the MHz range and a superconducting quantum interference device (SQUID), interfaced to high-bandwidth field programmable gate array (FPGA)-based electronics for digital signal processing and low-latency feedback.

KEYWORDS: Cryogenic calorimeters, Superconducting detectors, Transition-edge sensors, Neutrinoless double-beta decay detectors, Multiplexed readout, Digital frequency domain multiplexing, FPGAs

Contents

1	Introduction	1
2	Frequency domain multiplexing TES readout	3
3	Cold components	4
3.1	Resonator board	4
3.2	Resonator chip design	5
4	Room temperature readout	6
4.1	The McGill ICEboard electronics	6
4.2	New high-bandwidth fMUX firmware	7
5	Multiplexing demonstration	10
6	Conclusion and outlook	13

1 Introduction

Cryogenic experiments searching for neutrinoless double beta decay employ increasingly large detector masses and require faster cryogenic sensors to discriminate between the expected signal and the different types of background. Transition edge sensors (TESs), which are prolifically used in cosmic microwave background (CMB) telescopes (e.g. [1–4]), are a promising technology for both calorimeters and light detectors [5]. Large arrays of TESs have been used in rare event searches for dark matter [6]. However, when operating at cryogenic temperatures of about 10 mK, the thermal load from the wiring used to instrument these detectors presents an architectural challenge. Multiplexing the readout becomes necessary with $\mathcal{O}(1000)$ detector channels. Additionally, reducing the cabling and material close to the detector is beneficial for radioactive background reduction.

This work discusses the multiplexed readout developed for TES detectors that aim to measure light coming from particle interactions in scintillating crystals. Such an application is particularly relevant for the CUPID (CUORE Upgrade with Particle IDentification) experiment [7]. CUPID aims to detect $0\nu\beta\beta$ from ^{100}Mo , with the signal appearing as a monoenergetic peak at the Q-value of the reaction (3034 keV) above a constant background. A large fraction of this background, induced by alpha particles, is discriminated by the CUPID heat/light double readout technology, employing scintillating $\text{Li}_2^{100}\text{MoO}_4$ (LMO) crystals coupled to light detectors. However, due to the relatively short half-life of the $2\nu\beta\beta$ decay of ^{100}Mo , $T_{1/2}^{2\nu} \simeq 7.06 \times 10^{18}$ yr [8], the pileup coming from this process would become the largest source of background in the region of interest (ROI) for CUPID, contributing up to half of the total expected background budget [7]. Consequently, this is one of the most critical items to address to increase the sensitivity of the experiment.

Timing pileup consists of events that are coincident in a time window shorter than the length of a single pulse. As this background is originating from the same isotope as the process of interest, the only way to reduce it is to discriminate it from single interactions with faster detectors. Although CUPID’s baseline design [7] utilizes light detectors with Neganov-Trofimov-Luke amplification readout through NTD sensors [9], multiplexed TESs are an alternative readout under development, and are expected to be the design choice for the future tonne-scale upgrade of the experiment [10]. TESs are one order of magnitude faster than NTDs ($\mathcal{O}(100\ \mu\text{s})$ vs $\mathcal{O}(\text{ms})$) [5, 9] and allow for a significantly better rejection of $2\nu\beta\beta$ pileup events, crucial for tonne-scale $0\nu\beta\beta$ searches.

We consider the following requirements for a CUPID-like TES detector readout:

- Signal bandwidth in the kHz range, in order to capture the $\mathcal{O}(100\ \mu\text{s})$ risetime of TES sensors and allow for pulse shape discrimination techniques;
- TES detectors require low series impedance readout and cabling to maintain stability of the electro-thermal feedback loop. Superconducting quantum interference devices (SQUIDs) are therefore used to readout and amplify the signal;
- The technology needs to be scalable to tonne-scale calorimeters that will employ thousands of channels;
- A multiplexing factor of 10-15 is sufficient for the CUPID cryostat to achieve sufficiently low thermal load at 10 mK. Keeping the multiplexing factor low limits the number of channels that would be lost in case of hardware or wiring failures;
- Radioactivity constraints require having as little material as possible close to the detector, meaning that the readout hardware has to be kept as far as possible from the TESs. For the first phase of CUPID, the experiment will use the current CUORE cryostat. The distance between the SQUIDs on the still stage and the detectors placed below the lead shield on the mixing chamber is on the order of 1-2 m, depending on where the detector is located within the experimental volume [11].

One of the main challenges compared to CMB telescope implementations using this technology is adapting the design to higher signal bandwidth. In CUPID, the scintillation light signals are orders of magnitude faster than those measured in CMB experiments. This requires a frequency domain multiplexing (fMUX) readout system and thus a resonant circuit with resonance widths on the order of tens of kHz. A second important difference is minimizing material close to the TES to reduce radioactive contamination, which would otherwise mask the rare event signal. Consequently, the cabling between the TES and the SQUID amplification stage needs to be longer, which can shift the detector resonance frequencies and is potentially more susceptible to noise pickup from the environment. In addition, due to the size of the CUPID cryostat, the cabling between the SQUID and the warm readout is much longer than in CMB experiments, which inserts signal attenuation that negatively affects the signal-to-noise ratio. The noise performance of the designed fMUX system is a fairly rich and nontrivial topic, which we discuss in a separate paper – see [12].

The structure of this paper is as follows. In section 2 we present the general working principle of the readout system. Section 3 focuses on the cryogenic components, while the warm electronics and

the associated field programmable gate array (FPGA) firmware are described in detail in section 4. In section 5 we report the first measurements carried out to validate the system. Section 6 concludes the paper and provides some outlook on future work.

2 Frequency domain multiplexing TES readout

The fMUX readout system presented here is in principle very similar to the one developed for CMB experiments like POLARBEAR-2, Simons Array, SPT-3G and LiteBIRD (see Ref. [13]), but adapted to cryogenic calorimetric experiments – figure 1 shows the system configuration. It implements 10 detector channels, where each TES is placed in series with an LC circuit with a unique resonant frequency between 1-5 MHz. The readout electronics generate a comb of carrier tones, providing a voltage bias for each individual TES detector, which are kept at their operating points via electro-thermal feedback [14]. The resulting bias currents are summed together and inductively coupled to a DC-SQUID, which acts as a transimpedance amplifier. When energy is deposited in a TES, its resistance changes, creating an amplitude modulation of the current at its associated LC filter frequency, which is digitized and demodulated by the readout electronics. Our implementation of the fMUX TES readout, like its CMB predecessor, also makes use of Digital Active Nulling – DAN [15], which dynamically injects a current along the nullder line that cancels the current flowing through the SQUID input coil, keeping the SQUID in the linear working regime. When DAN is active, all the science signal is therefore encoded in the nullder line (see figure 1), while the demod line coming from the SQUID amplifier only contains the residuals (i.e., control error) that serve as an input to the DAN controller. The tone generation, demodulation, and the DAN loop are implemented digitally on McGill’s FPGA-based "ICEboard" digital signal processing platform, described in more detail in section 4.

There has been some effort in the past to convert the CMB fMUX readout to a high-bandwidth version for superconducting gamma-ray spectrometers [16]. However, the hardware (both cold and warm) back then was much less sophisticated, the TES bias frequencies were lower, and most importantly, SQUID nulling was static, i.e. only the carrier tones were nulled out, while the sidebands were still carried over onto the demod line. Since the linearity of the detector readout is crucial for achieving the high energy resolution needed for CUPID, the DAN scheme in this modern implementation of high-bandwidth fMUX is a substantial step forward.

We tested the system in an Oxford Triton 400 dilution cryostat at UC Berkeley. The TESs employed for this demonstration are IrPt bilayer devices with a critical temperature, T_c , of 35 mK or 55 mK, described in [5]. They are deposited on high-purity Si wafers of 500 μm thickness and diced to $45 \times 45 \text{ mm}^2$ in size. The TESs were installed on the mixing chamber stage at 12 mK, while the LC filters and the SQUID are on two chips glued on a printed circuit board (PCB) on the still stage at slightly below 700 mK – see figure 1. This cryogenic resonator board, together with the superconductive cabling, is described in more detail in section 3 below.

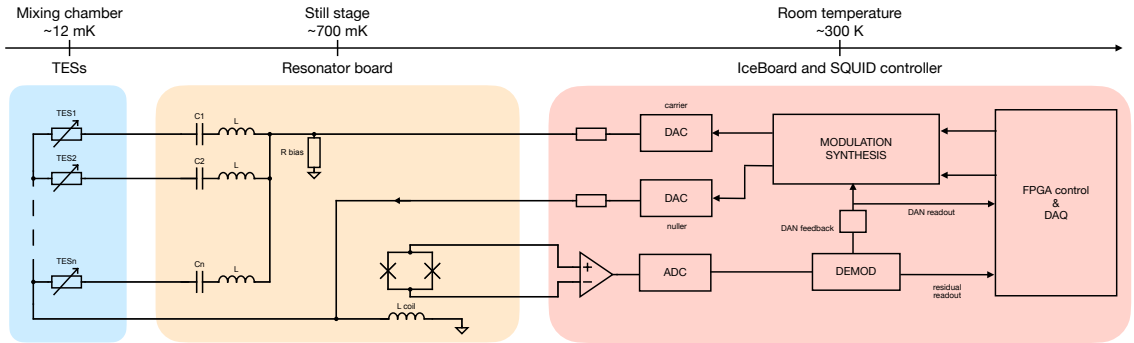


Figure 1. Simplified circuit schematic of a single module of the fMUX TES readout. The colours indicate the components installed at different temperatures inside and outside the cryostat. The FPGA-based ICEboard sits at room temperature with the carrier and nulier DACs, the demod ADC, and the SQUID controller circuitry. The still stage at ~ 700 mK hosts the LC resonator board and the SQUID, while the TESs are located at the mixing chamber stage at around 12 mK. The TESs are voltage biased with carrier tones and their respective currents summed up at the SQUID summing junction. When the digital active nulling (DAN) is active, these currents flow predominantly through the nulier line instead of the SQUID input coil, keeping the SQUID in the linear operating regime. Figure from [12].

3 Cold components

3.1 Resonator board

The multiplexing PCB, also referred to as the resonator board (highlighted in yellow in figure 1), hosts both the resonator chip and a NIST SA13a DC-SQUID array [17]. The two chips are attached to the PCB with rubber cement and connected to the board via $25\ \mu\text{m}$ aluminum wire bonds (see figure 2). The PCB is patterned with superconducting aluminum traces with copper added selectively to the pads, allowing for soldering to the readout wiring and other components with very low loss. A $5\ \Omega$ snubber resistor (R_1) is soldered in parallel with the SQUID input coil to remove non-linearities in the $V(\Phi)$ curves, which can occur when operating SQUID arrays at low temperatures [18, 19]. A $100\ \Omega$ resistor (R_2) serves as a heater in case it is necessary to warm the SQUID from its superconducting to its normal state. This can be useful if the SQUID has any remaining trapped flux acquired during cooldown. Lastly, a $20\ \text{m}\Omega$ bias resistor (R_3) provides a frequency-independent voltage bias for the TESs.

The resonator board is enclosed in a high purity (5N) aluminum box that, in its superconducting state, protects the board from external magnetic fields. We wrapped the box in a layer of Metglas® magnetic foil, providing further shielding from the external magnetic field. The assembly is thermalized to the still stage (~ 700 mK) through a copper rod.

Thermalizing TESs to the mixing chamber, while the resonator chip and the SQUID are mounted on the still stage, poses a challenge for cabling. Ideally these components would be as close to each other as possible to minimize attenuation and parasitic effects before the amplification of the signal. This ideal case is better realized in systems implemented for CMB telescopes, where both the TES and the readout SQUID can operate at the same temperature (about a couple hundreds of mK) [19]. However, because this readout system is intended for low-background cryogenic

calorimeters, the non-active material close to the detectors must be minimized and the detectors themselves must be as cold as possible (12 mK), where SQUIDs cannot reliably operate. To address this distance between the TESs and the SQUID, we use superconducting NbTi twisted pair cables to connect the TESs to the resonator board, where low-loss, fine-pitch Omnetics NanoD connectors make the connection to selective copper pads. On the TES side of the circuit, the connections are limited to NanoD connectors, Al solder pads, and Al wirebonds to keep the parasitic resistance as low as possible. The same choice of connectors and cables is also used to interface the SQUID with room temperature control and readout. As seen later in section 5, the stray inductance of this cabling will affect the performance of the system.

3.2 Resonator chip design

Our LC resonator chip is adapted from the POLARBEAR2 design [20], modified by the unique physics constraints of CUPID. The TESs developed for a CUPID-like experiment have an expected normal resistance of $\sim 1 \Omega$ and a time constant $\tau_{TES} \sim 50 \mu\text{s}$, roughly 200 times faster than POLARBEAR2. To ensure the stability of the calorimeter, τ_{TES} needs to exceed the electrical time constant of the RLC circuit, τ_e , according to the relation [20]:

$$\tau_{TES} > 5.8 \cdot \tau_e \simeq 5.8 \cdot \frac{2L}{R_{TES}}. \quad (3.1)$$

From this we obtain the desired value for the inductance of the resonator, $L < 4.3 \mu\text{H}$. For our design, we chose to fix the inductance value for all the resonators at $L = 4 \mu\text{H}$, and we vary the value of the coupled capacitance. This also keeps the bandwidth of each resonance constant. Considering a readout frequency of 1-5 MHz, we need capacitors on the order of $O(1 \text{ nF})$.

The spacing between resonances follows the constraint of $\Delta f > 0.3 \text{ MHz}$, in order to reduce the crosstalk, XT , to a sub-percentage level. The dominant component for the crosstalk is the leakage current between neighboring resonances, with a contribution given by [20]

$$XT_{lc} = \left(\frac{R_{TES}}{4\pi\Delta f L} \right)^2, \quad (3.2)$$

which is designed to be less than 0.4 % in our system. Another consideration when choosing the spacing of the resonances is minimizing the effect of intermodulation distortion (IMD) products between the carrier tones. Given that the distance to the second closest resonance is at least 0.6 MHz with a $XT_{lc} < 0.1 \%$, we consider only the third order intermodulation effects between adjacent resonances. Thus, we space the resonant frequencies non-linearly to avoid the intermodulation distortion peaks, and with a resonance bandwidth of 40 kHz. The selected resonant frequencies with the associated capacitances are reported in table 1.

The resonator chip is fabricated on a silicon substrate with a lithographed aluminum layer of planar, spiral inductors in series with interdigitated (IDC) capacitors. The resonators are placed next to each other in one row. To further reduce crosstalk, resonances close in frequency are spatially distant on the chip. The spatial ordering of the resonances on the chip is reported in the last column of table 1, where the seventh resonance (3.488 MHz) corresponds to the leftmost capacitor in figure 2. In addition, adjacent resonators have their respective inductors on alternating sides of the capacitors to avoid mutual inductance.

Table 1. Resonances chosen for the design of the 10-channel resonator chip, with the corresponding capacitance needed when using an inductance of $4\ \mu\text{H}$.

No.	Resonance frequency [MHz]	Capacitance [nF]	Order on chip
1	1.472	2.932	3
2	1.772	2.017	6
3	2.144	1.378	9
4	2.444	1.060	2
5	2.816	0.799	5
6	3.166	0.652	8
7	3.488	0.521	1
8	3.788	0.441	4
9	4.160	0.366	10
10	4.460	0.318	7

The inductor is identical for each resonator and is made of 60 square turns with a trace gap and width of $4\ \mu\text{m}$, resulting in a side dimension of $1400\ \mu\text{m}$. The capacitors are made of two vertical pads with horizontal fingers in between, with a trace gap and width of $2\ \mu\text{m}$. This is done to reduce the size of the capacitors so that the chip is as compact as possible. Each capacitor is connected to its inductor on one side and the bonding pad on the other, that will be connected to the TES. The size of the resonator chip is $38.4\times36.9\ \text{mm}^2$, with an additional millimeter on each side for the dicing lines used during production. The dimensions of the entire resonator board are $70\times60\ \text{mm}^2$, which is small enough to fit on the still stage.

4 Room temperature readout

4.1 The McGill ICEboard electronics

For the digital frequency multiplexing control and readout of the cryogenic detectors, we are using the McGill Cosmology Instrumentation Laboratory’s ICEboard electronics [21], shown in figure 3. The motherboard, originally developed for CMB experiments, is based on a high-performance Xilinx Kintex-7 FPGA, which runs the digital signal processing firmware for TES readout [13]. This includes synthesizing and demodulating readout tones, the DAN control loop, and the downsampling and streaming of science data, which are sent out through a 1 Gb/s Ethernet link. The board also contains an ARM processor running a Linux operating system, which serves as a low-level interface between the FPGA and the host computer.

The digital waveforms are converted to analog signals and the analog signals returning from the cryostat are digitized using 16-bit 20 Msps ADCs and DACs on the two custom FPGA mezzanine cards (FMCs) mounted on the ICEboard. The mezzanines connect to a separate SQUID Controller board [13], also made by McGill, connecting to the cryostat. The hardware supports the readout of up to 8 modules (each containing a SQUID and an array of detectors), although only one is currently enabled by the CUPID firmware due to bandwidth limitations specific to the present configuration of the ARM’s Ethernet transceiver, discussed in more detail in section 4.2. The Iceboard has



Figure 2. Cryogenic resonator board with the LC resonator chip in the center and the NIST SA13 SQUID at the bottom, together with the snubber (R1) and bias (R3) chip resistors. The board is placed in an aluminum box at the still stage at ~ 700 mK inside the cryostat.

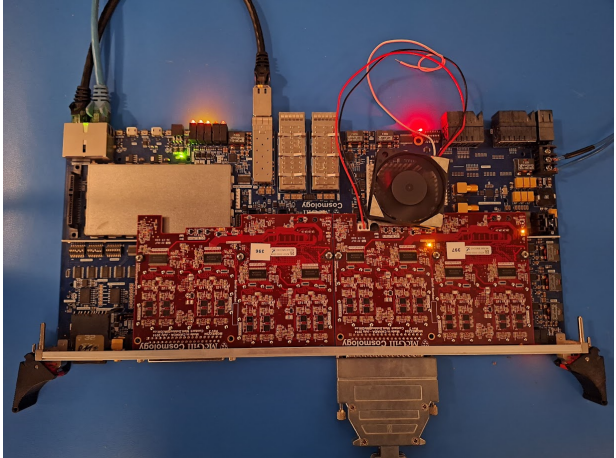


Figure 3. McGill's ICEboard warm readout electronics. The blue motherboard hosts the FPGA for digital processing, while the red mezzanine cards contain the ADCs and DACs. The DB-37 cable at the bottom connects to the SQUID Controller Board (not shown here), while the Ethernet cable at the top interfaces with the host PC. The board supports the readout of up to 8 fMUX modules, although we only use one in this work.

high-speed serial links available (SFP or QSFP directly from the FPGA), so this will not be an issue in the long term.

4.2 New high-bandwidth fMUX firmware

30 ICE boards are currently deployed at the South Pole Telescope (SPT) in Antarctica, where they read out approximately 16,000 TES detectors for the SPT-3G experiment [4, 22], scanning the CMB sky. For CUPID TES readout, we are using the exact same warm hardware as for SPT-3G; however, the science requirements are very different. While the SPT slowly scans the sky, requiring a low sampling rate, CUPID must read out its detectors much faster to avoid $2\nu\beta\beta$ pileup events. Therefore, new fast readout firmware was designed at McGill to meet its science goals, specifically for CUPID. We present its inner workings below.

While the SPT firmware [13] is optimized for high multiplexing ratios at low sample rates, CUPID does the opposite. The new firmware increases the output data rate to 156 ksps, up by three orders of magnitude compared to 153 sps for SPT-3G. On the other hand, the fMUX ratio is reduced to 10x, down from 128x for SPT-3G. The SPT firmware achieves such high multiplexing factors through the use of polyphase filter banks (PFBs), a very efficient way of splitting the band into multiple narrow channels. Since the requirements for CUPID are the opposite (only a few very wide channels), the PFBs have been removed, significantly reducing the firmware footprint of the design. The architecture of the new firmware is shown in figure 4.

The firmware signal processing works as follows. Raw data comes in from the analog-to-digital converter (ADC) at 20 Msps and is quadrature demodulated to baseband by mixing it with the local oscillator (LO) signal, which generates the tones for all 10 channels using Direct Digital Synthesis

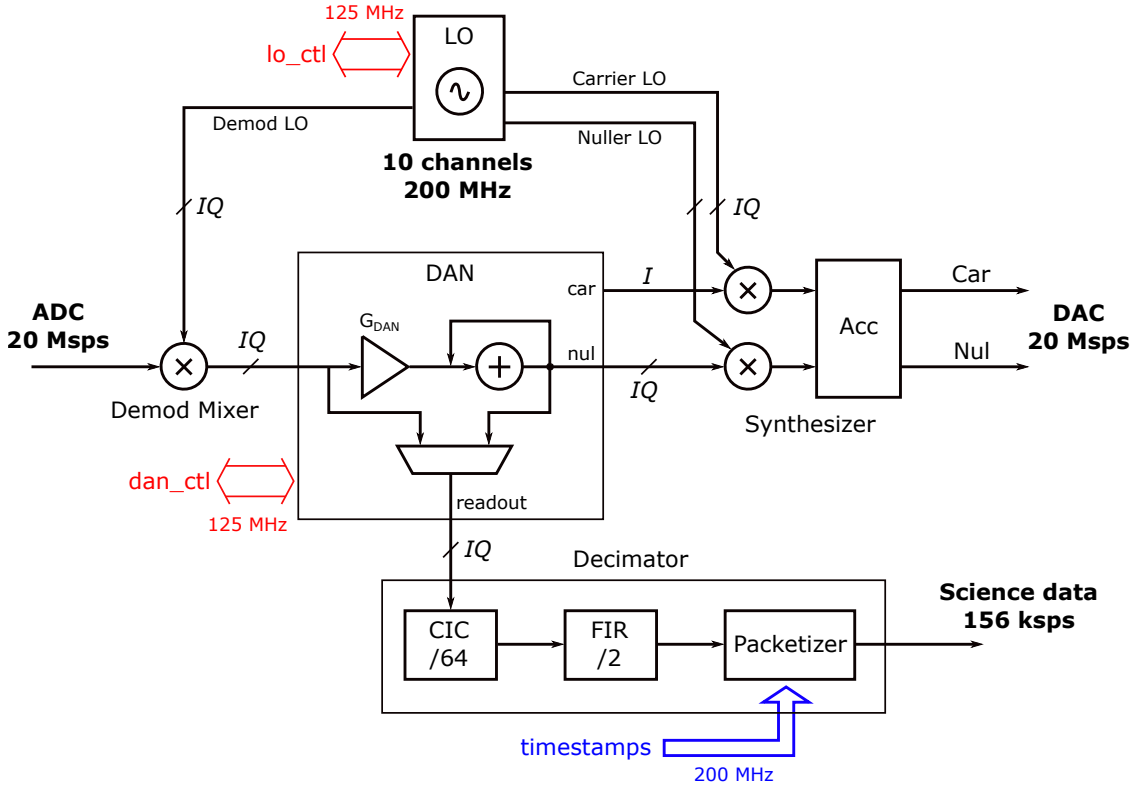


Figure 4. Core architecture of the high-bandwidth, 10-channel fMUX firmware module for CUPID, clocked at 200 MHz. The main difference compared to McGill’s SPT firmware [13] is the absence of polyphase filter banks (PFBs) and a new decimation path. The DAN loop remains the same, albeit it runs at a higher sampling rate. The operation of the firmware is controlled via 125 MHz control interfaces, marked in red, which ultimately connect to the ARM processor through an on-board SPI link. There is also a Global Positioning System (GPS)-derived input in IRIG-B format, which attaches timestamps to the data packets (in blue).

(DDS). Channel processing is time-multiplexed, corresponding to a system clock of 200 MHz (200 MHz/10 = 20 Msps). Turning to the synthesis side on the right of figure 4, a series of carrier and nul waveforms are generated by mixing their baseband amplitudes with the LO signals. The accumulator sums all of them together, creating a frequency comb at 20 Msps, which feeds the carrier and nul DACs (digital-to-analog converters).

The decimator downsamples the 20 Msps data to 312.5 ksps (/64) with a 6-stage cascaded integrator-comb (CIC) filter [23] with an anti-aliasing rejection of more than -60 dB. Since CICs are known to have a significant magnitude droop in the passband, a compensating FIR (finite impulse response) decimator (/2) follows, flattening the passband for the final science output data rate of 156.25 ksps. The channelized data are packetized and sent off the FPGA to the ARM processor over Ethernet.

At the core of the readout module is the DAN control loop [15], which actively adjusts the nul amplitude to cancel any signal at the input (see also figure 1). When DAN is enabled, the nul line encodes the science data, so it is the one being sampled and packetized instead of the

demod line. The DAN module is an integral controller with an adjustable digital gain G_{DAN} , which sets the aggressiveness of the feedback. The total feedback loopgain, K_0 , is the product of the set gain G_{DAN} and all other gains in the external nuller-demod circuit loop, here denoted as "loopgain" LG .

$$K_0 = G_{DAN} \times LG \quad (4.1)$$

The higher the feedback gain K_0 , the faster the nuller will respond to changes at the SQUID input coil. Specifically, the signal bandwidth is linearly proportional to K_0 , and in general, we would like the bandwidth to be as high as possible. However, there is an upper limit to K_0 , above which *antinulling* occurs and the control loop becomes unstable, a phenomenon discussed in detail in Ref. [24]. Two factors are limiting this. The first is the loop latency, which was estimated to be $\sim 2.2 \mu\text{s}$ for this system, a significant improvement from $14 \mu\text{s}$ for the SPT firmware (due to removing the polyphase filter banks – PFBs). The second limiting factor is due to loopgain nonuniformity, which was observed during operation and is unique to high-bandwidth TES readout. Since the readout Nyquist frequency is high (78 kHz), the resonator impedance varies significantly within it, and so does the loopgain LG (due to the varying nuller current sharing factor – see [12]). In other words, LG increases at frequencies away from the center of the resonance. This causes the points at the edge of the Nyquist region to enter the antinulling regime. Since only a single value of G_{DAN} can be programmed per channel, the entire channel's digital gain must be set more conservatively. Using the current firmware and readout configuration, the highest attained safe DAN readout bandwidth is around 3 kHz, corresponding to detector risetimes of $\sim 120 \mu\text{s}$. To improve this, one could either widen the LC resonances (which will adversely affect crosstalk), implement a higher-order DAN controller, or reduce the output sample rate of the system.

The single readout module CUPID firmware was implemented on the Iceboard's Kintex-7 420T FPGA using Xilinx Vivado 2021.2 ML. The reported firmware utilization is 4.0 % of Lookup Tables (LUTs), 3.1 % of Registers (total Slice utilization 7.2 %), 3.7 % of Block Random-Access Memory (BRAMs) and 2.7 % of Digital Signal Processing (DSP) blocks with an estimated on-chip power of merely 2 W. Therefore, the design is easily scalable up to 8 modules, which is the physical number of hardware readout modules on the Iceboard.

The issue for the time being is the ARM-based network bandwidth, which cannot handle that many UDP packets. A single IQ datapoint is a 64-bit word, times 10 channels at 156250 sps equals to 100 Mbit/s, not taking into account the structure of our UDP packets which adds another 10% overhead, so a total datarate of ~ 110 Mbit/s per module. The packets are sent from the FPGA to the on-board ARM processor through a short UTP loopback, where a special process runs that routes the packets to the host computer via a separate 1.0 Gbps Ethernet port. The reason behind this configuration is that the ARM Linux system hosts a set of C-based algorithms which serve as a low-level control interface between the firmware and the host computer, and sometimes these algorithms need access to output data. This process-based packet routing has a bottleneck at around 150 Mbps, limiting the firmware to only one active 10x module. The solution to this is known and successfully implemented in McGill's RF-ICE [25] GHz multiplexing Iceboard system, where the data rates can go above 500 Mbps, which would enable the implementation of 4–6 modules. However, for the full 8-module system, the 1.0 Gbps Ethernet interface hard limit will become a problem, prompting the transition to on-board 10 Gbps links [21], used by default on Iceboards

deployed at the CHIME radio telescope [26].

We also successfully implemented and tested a 15x frequency multiplexing version of the firmware, using various modifications that enabled increasing the clock frequency to 300 MHz. However, similarly to the 8-module readout, it is limited by network bandwidth constraints. In the future, it is essential to rethink how we offload data from CUPID Iceboards to unlock the full scalability of this high-bandwidth TES fMUX readout firmware.

5 Multiplexing demonstration

To validate and characterize the system, we first carried out measurements replacing the TES array with a board with a "dummy payload" of 10 surface mount (SMD) $0.5\ \Omega$ resistors, attached to the resonator board and thermalized to the still stage at 700 mK. This allowed us to perform the basic multiplexing and noise characterization [12] of the system first without the complications related to operating TES detectors.

The top panel of figure 5 shows the network analysis of the setup from 1 to 5 MHz, performed with the Iceboard. The plot is showing the "DAN network analysis", which is produced by physically measuring the carrier transfer function and dividing it by the nullder transfer function. This eliminates the impedance of the SQUID input coil from the expression, corresponding to the true comb admittance when DAN is operating. [27] The TESs (or in this case regular resistors) are subsequently biased at the maxima of such network analysis. All ten resonances are visible, with an average shift towards lower frequencies of $(4.5\pm0.2)\%$ from the design (middle panel). This corresponds to an increase of the LC constant of the resonators of $(9.6\pm0.5)\%$, indicating the presence of parasitic components, mostly inductance from the TES-SQUID NbTi wiring. The shift in frequency changes the relative distance among the resonances, potentially affecting crosstalk, XT_{lc} . The bottom panel shows the design and measured resonance frequencies and different XT_{lc} levels. While most resonance pairs still satisfy the design requirement of $XT_{lc} \leq 0.4\%$, three pairs have a $XT_{lc} \leq 0.6\%$.

We have also measured the readout noise of the system with DAN enabled, corresponding to TES readout currents on the nullder line – see figure 6. The spectra have a noise roll-off at 3 kHz, matching the bandwidth of the DAN loop discussed earlier. This demonstrates the readout bandwidth corresponding to a $120\ \mu\text{s}$ signal risetime detection capability, meeting the design requirement. The measured white noise levels across the DAN bandwidth were $20 - 50\ \frac{\text{pA}}{\sqrt{\text{Hz}}}$ at the SQUID summing junction, depending on the bias frequency (noise generally rises with frequency). We provide a detailed investigation of the noise in [12]. Briefly, various engineering choices contribute to higher than anticipated white noise levels. The sources of the noise are understood and will be addressed in future implementations of the system.

We notice some intermodulation distortion (IMD) products in the spectra, which form between the readout tones and the 20 MHz sampling clock, not considered at the design stage. These spikes are not problematic for a CUPID-type experiment, since the pulse information is encoded in the entire readout bandwidth. With additional tone frequency scheduling in future design iterations, most IMD spikes can be avoided, and any remaining ones can be notched out in post-processing of the data.

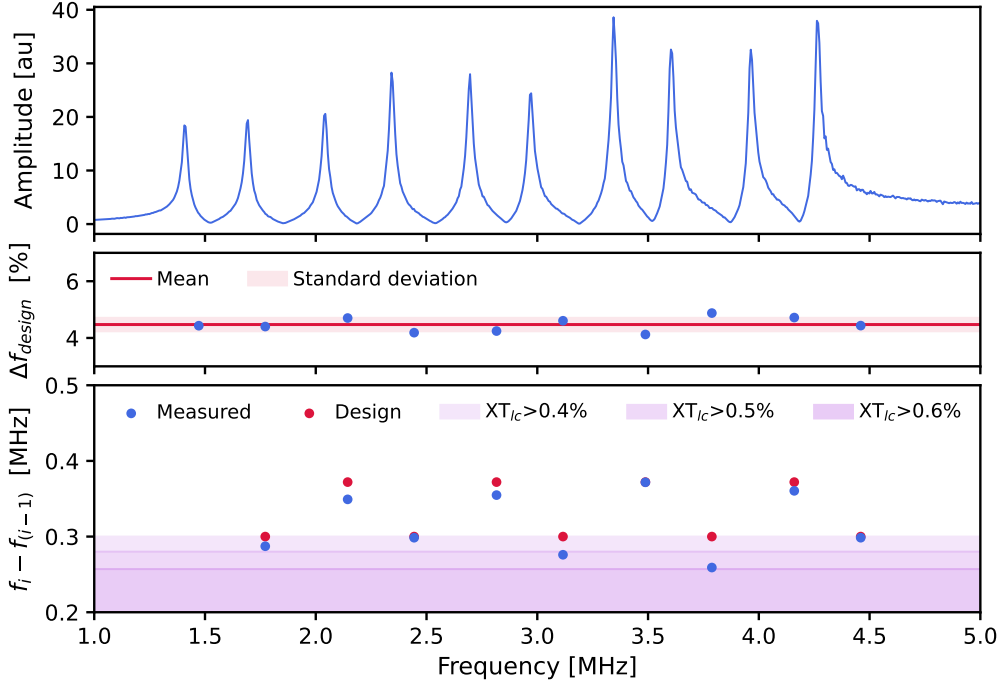


Figure 5. Top panel: DAN network analysis of the system with 0.5Ω SMD resistors. All 10 resonances are visible, with peaks corresponding to chosen detector bias points. Middle panel: shift in frequency between the measured resonance values (in the top panel) and the design ones, with the point x -axis corresponding to design resonance frequencies. Mean and standard deviation are shown by the solid line and the shaded red region, respectively. Bottom panel: the distance between neighboring resonances for measured (blue) and design (red) values – note that the red and blue dots overlap in three cases. The contribution of the leakage cross-talk is overlaid in shades of purple.

Lastly, we tested the system with an array of 9 TESs installed at 12 mK, developed specifically for CUPID in [5] and briefly introduced in section 2. We performed a DAN network analysis at 20 mK and 75 mK (below and above transition) to visualize the admittance variation of the resonances between the superconductive and normal regimes. We observed 6 devices transitioning. The DAN was enabled for all TES channels above their transition temperatures, and high bias voltages were programmed to keep them in the normal regime. After the mixing stage was lowered below T_c , the bias voltages were slowly reduced to lower the TESs into transition – see figure 7. We could estimate a series parasitic impedance between $50\text{ m}\Omega$ and $75\text{ m}\Omega$ on the TES lines from these load curves. This impedance affects the shape of the pulses; in particular, it increases the risetimes, reducing the pileup discrimination capabilities of the TES.

To demonstrate calorimetric reconstruction of optical photons with the developed fMUX readout, as is necessary to discriminate backgrounds in CUPID, we routed a cryogenic diffusive optical fiber down to the TES array at 12 mK. The fiber mates to the vacuum feedthrough at 300 K, which connects to another segment of fiber leading to an LED at room temperature. A signal

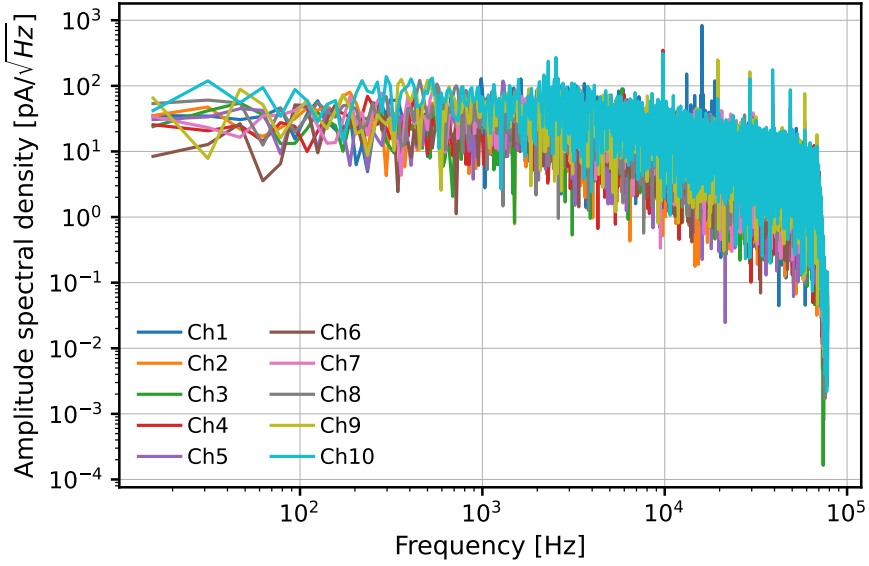


Figure 6. Noise spectra of the 10 active channels with DAN enabled, measured as current on the nulier line – see figure 1. The 3 kHz white noise roll-off is clearly visible, demonstrating the required readout bandwidth. The spikes in the high frequency part of the spectrum are IMD products between the readout tones and the 20 MHz ADC/DAC clock. For the discussion of white noise amplitudes, see Ref [12].

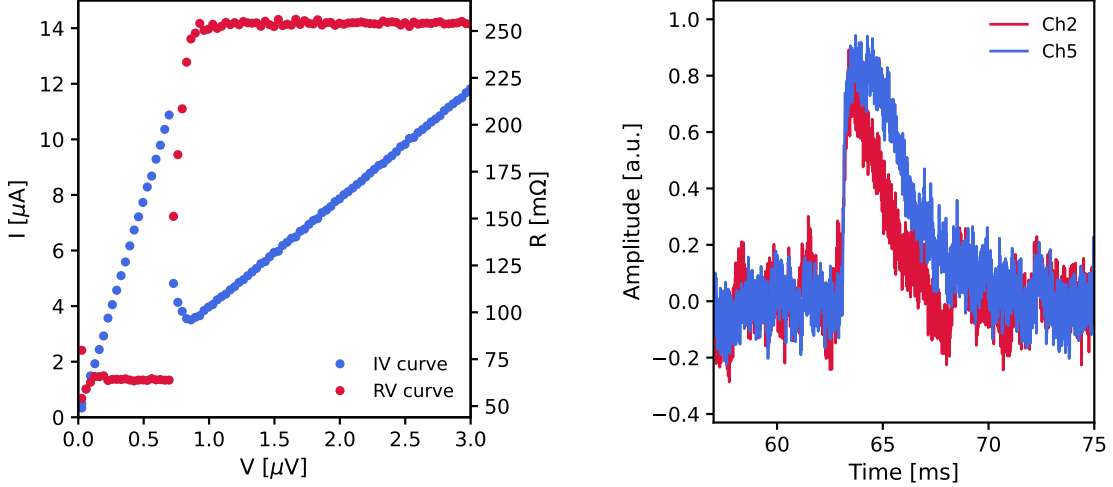


Figure 7. Current (I) and measured resistance (R) of the fifth TES as a function of bias voltage (V) as the bolometers are lowered into transition. Residual parasitic impedance (about 70 mΩ) is clearly visible in the superconducting state.

Figure 8. Example of a short LED pulse picked up by two TES devices via a semi-transparent optic fiber inside the cryostat.

generator drives the LED with a square pulse train, generating optical photons with an intensity proportional to the pulse width. The pulse width of the signal generator was tuned to keep the TESs below their saturation limit. We acquired data on two TES devices, shown in figure 8, where we

can see demodulated time streams showing coincident pulses picked up by both TESs.

6 Conclusion and outlook

We developed a frequency domain multiplexing readout system for TESs with a signal bandwidth in the kHz range, as required by the next generation of cryogenic calorimetric double beta decay experiments. The readout system is adapted from CMB experiments, namely POLARBEAR2 and SPT-3G. The higher readout bandwidth required a new design of the LC resonator board and a new firmware for the FPGA signal processing motherboard. The installation in the cryostat and the cabling were modified to reduce the heat load on the mixing chamber at ~ 12 mK and to minimize the material close to the detector, as required by rare event search experiments. The new system was successful in reading out multiplexed devices, which respond to light pulses. Residual parasitic impedance was measured, originating from cables and connectors. Although some further optimization is required, the system meets the physics requirements for next-generation rare-event cryogenic calorimeters and is scalable to higher channel counts. The multiplexed readout developed herein facilitates the deployment of thousands of TES sensor channels, a scale crucial for future tonne-scale detectors.

References

- [1] M.A. Dobbs et al., *Frequency multiplexed superconducting quantum interference device readout of large bolometer arrays for cosmic microwave background measurements*, *Rev. Sci. Instrum.* **83** (2012) 073113.
- [2] POLARBEAR collaboration, *Development of readout electronics for POLARBEAR-2 Cosmic Microwave Background experiment*, *J. Low Temp. Phys.* **184** (2016) 512.
- [3] BICEP2, KECK ARRAY, SPIDER collaboration, *Antenna-coupled TES bolometers used in BICEP2, Keck array, and SPIDER*, *Astrophys. J.* **812** (2015) 176.
- [4] SPT-3G collaboration, *The Design and Integrated Performance of SPT-3G*, *Astrophys. J. Supp.* **258** (2022) 42.
- [5] V. Singh et al., *Large-area photon calorimeter with Ir-Pt bilayer transition-edge sensor for the CUPID experiment*, *Phys. Rev. Applied* **20** (2023) 064017.
- [6] M. Pyle, P.L. Brink, B. Cabrera, J.P. Castle, P. Colling, C.L. Chang et al., *Quasiparticle propagation in aluminum fins and tungsten TES dynamics in the CDMS ZIP detector*, *Nucl. Instrum. Meth. A* **559** (2006) 405.
- [7] CUPID collaboration, *CUPID, the CUORE upgrade with particle identification*, *Eur. Phys. J. C* **85** (2025) 737.
- [8] A. Barabash, *Precise Half-Life Values for Two-Neutrino Double- β Decay: 2020 Review*, *Universe* **6** (2020) 159.
- [9] D.M. Chernyak et al., *Rejection of randomly coinciding events in $\text{Li}_2^{100}\text{MoO}_4$ scintillating bolometers using light detectors based on the Neganov–Luke effect*, *Eur. Phys. J. C* **77** (2017) 3.
- [10] CUPID collaboration, *Toward CUPID-IT*, [2203.08386](https://arxiv.org/abs/2203.08386).
- [11] C. Alduino et al., *The CUORE cryostat: An infrastructure for rare event searches at millikelvin temperatures*, *Cryogenics* **102** (2019) 9.

- [12] M. Adamič, J. Camilleri, C. Capelli, M. Dobbs, T. Elleflot, Y.G. Kolomensky et al., *Readout noise of digital frequency multiplexed TES detectors for CUPID*, *IEEE Trans. Nucl. Sci.* (2025) 1.
- [13] A.N. Bender et al., *Digital frequency domain multiplexing readout electronics for the next generation of millimeter telescopes*, *Proc. SPIE Int. Soc. Opt. Eng.* **9153** (2014) 91531A.
- [14] K. Irwin and G. Hilton, *Transition-edge sensors*, in *Cryogenic Particle Detection*, C. Enss, ed., (Berlin, Heidelberg), pp. 63–150, Springer Berlin Heidelberg (2005), [DOI](#).
- [15] T. de Haan, G. Smecher and M. Dobbs, *Improved Performance of TES Bolometers using Digital Feedback*, *Proc. SPIE Int. Soc. Opt. Eng.* **8452** (2012) 84520E.
- [16] J.G. Dreyer, K. Arnold, T.M. Lanting, M.A. Dobbs, S. Friedrich, A.T. Lee et al., *Frequency-domain multiplexed readout for superconducting gamma-ray detectors*, *IEEE Trans. Appl. Supercond.* **17** (2007) 633.
- [17] M. Silva-Feaver, K. Arnold, D. Barron, E.V. Denison, M. Dobbs, J. Groh et al., *Comparison of NIST SA13a and SA4b SQUID Array Amplifiers*, *J. Low Temp. Phys.* **193** (2018) 600.
- [18] M. Huber, P. Neil, R. Benson, D. Burns, A. Corey, C. Flynn et al., *DC SQUID series array amplifiers with 120 MHz bandwidth*, *IEEE Trans. Appl. Supercond.* **11** (2001) 1251.
- [19] T. Elleflot et al., *Low Noise Frequency-Domain Multiplexing of TES Bolometers Using SQUIDs at Sub-Kelvin Temperature*, *J. Low Temp. Phys.* **209** (2022) 693.
- [20] K. Rotermund, B. Barch, S. Chapman, K. Hattori, A. Lee, N. Palaio et al., *Planar Lithographed Superconducting LC Resonators for Frequency-Domain Multiplexed Readout Systems*, *J. Low Temp. Phys.* **184** (2016) 486.
- [21] K. Bandura et al., *ICE: a scalable, low-cost FPGA-based telescope signal processing and networking system*, *J. Astron. Inst.* **05** (2017) 1641005.
- [22] SPT-3G collaboration, *SPT-3G: A Next-Generation Cosmic Microwave Background Polarization Experiment on the South Pole Telescope*, *Proc. SPIE Int. Soc. Opt. Eng.* **9153** (2014) 91531P.
- [23] E. Hogenauer, *An economical class of digital filters for decimation and interpolation*, *IEEE Trans. Acoust., Speech, Signal Process.* **29** (1981) 155.
- [24] G. Smecher, T. de Haan, M. Dobbs and J. Montgomery, *Digital active nulling for frequency-multiplexed bolometer readout: Performance and latency*, [2207.11377](#).
- [25] M. Rouble, G. Smecher, A. Anderson, P.S. Barry, K. Dibert, M. Dobbs et al., *RF-ICE: large-scale gigahertz readout of frequency-multiplexed microwave kinetic inductance detectors*, *Proc. SPIE Int. Soc. Opt. Phot.* **12190** (2022) 1219024.
- [26] CHIME collaboration, *An Overview of CHIME, the Canadian Hydrogen Intensity Mapping Experiment*, *Astrophys. J. Supp.* **261** (2022) 29.
- [27] J. Montgomery, *Digital Frequency Domain Multiplexing readout: design and performance of the SPT-3G instrument and LiteBIRD satellite readout*, Ph.D. thesis, McGill University, Montreal, QC, Canada, November, 2020.